SAND2011-0934C
Proceedings of ASME 2011 International Design Engineering Technical Conference & Computers and Information in Engineering Conference
IDETC2011
August 28-31, 2011, Washington, DC, USA

DETC2011-XXXXX

A NEW APPROACH TO MODELING DISCRETE NONLINEAR CONSTRAINTS IN CONTINUOUS SYSTEMS: THE METHOD OF DISCONTINUOUS BASIS FUNCTIONS

M. R. Brake* **and D. J. Segalman**
Sandia National Laboratories†
P.O. Box 5800, Albuquerque, NM 87185

ABSTRACT

Solutions for analytical models of systems with nonlinear constraints have focused on exact methods for satisfying the constraint conditions. Exact methods often require that the constraint can be expressed in a piecewise-linear manner, and result in a series of mapping equations from one linear regime of the constraint to the next. Due to the complexity of these methods, exact methods are often limited to analyzing a small number of constraints for practical reasons. This paper proposes a new method for analyzing continuous systems with arbitrary nonlinear constraints by approximately satisfying the constraint conditions. Instead of dividing the constraints into multiple linear regimes, a discontinuous basis function is used to supplement the system's linear basis functions. As a result, precise contact times are not needed, enabling this method to be more computationally efficient than exact methods. While the discontinuous basis functions are continuous in displacement, their derivatives contain discontinuities that allow for the nonlinear forces to be accounted for with the assumption that the nonlinear constraints are able to be modeled in a discrete manner. Since each nonlinear constraint requires only one associated discontinuous basis function, this method is easily expanded to handle large numbers of constraints. In order to illustrate the application of this method, an example with a pinned-pinned beam is presented.

*Corresponding author; mrbrake@sandia.gov

†Sandia National Laboratories is a multiprogram laboratory operated by Sandia Corporation, a Lockheed Martin Company, for the United States Department of Energy's National Nuclear Security Administration under Contract DE-AC04-94-AL85000.

1 Introduction

Nonlinearities are pervasive in the engineering problems that are common today; however, either the suite of analytical tools to efficiently study them often require significant approximations or simplifications, or the resulting simulations are very computationally expensive. Systems with nonlinear constraints include joints in large structures [1, 2], gears with backlash [3, 4], steam generator tubes in nuclear power plants [5,6], rotating shafts with cracks [7], and fluid conveying pipes with supports [8,9] amongst many other applications [10–12]. Typically, these nonlinearities are approximated by piecewise linear constraints. The discontinuities inherent in piecewise linear models have spurred research to smooth the force-deflection profile using a sigmoid function [13]. Other types of nonlinearties include Hertzian contact and coefficient of restitution models [14–16], cubic springs [9, 17], and Iwan friction models [18, 19].

The existing analytical studies of nonlinearities in continuous systems is limited for several reasons. For piecewise linear systems, a number of modal mapping methods exist that calculate the mode shapes of the system in each regime of the piecewise linear nonlinearity and then use the orthogonality of the mode shapes to map the displacement of the system across the point of nonlinearity [5, 20–22]. These methods, though, are often constrained in the order of the system [20,21] or the permissable parameter spaces [5, 22]. A recent approach has eliminated these constraints by proposing a mapping method based on the L_2 norm of the system [23]; however, in all cases, the limiting factor for computational time is finding the exact moment in time that the system transitions from one regime of the piecewise lin-

ear constraint to another. For other types of nonlinear constraints in continuous systems, such as Hertzian contact, only numerical studies (such as finite difference, finite element, or other approximate methods) exist in the literature.

The method proposed in Section 2 incorporates the effects of the nonlinear constraints by using a set of discontinuous basis functions. This approach is able to avoid the pitfalls encountered in prior methods. Additionally, because it does not involve switching between the various regimes of a nonlinearity, it is computationally efficient as it does not have to find exact switching times. This method originated in the study of large, discrete (finite element) systems with joints [24, 25]. This method has proven effective in analyzing discrete systems with arbitrary constraints; however, there has previously been no obvious approach for applying it to continuous systems. In Section 3, the method is applied to a pinned-pinned beam system as an illustrative example of its capabilities. Both piecewise-linear and piecewise-nonlinear constraints are used, and the extension of the method to multiple constraints is also discussed and illustratively shown.

2 The Discontinuous Basis Function Method

Given a continuous system with position vector $\underset{\sim}{x}$, time t, displacement $w(\underset{\sim}{x},t)$, and location of the N_L nonlinear constraints $\{\underset{\sim}{\ell}_1,\ldots,\underset{\sim}{\ell}_{N_L}\}$ in the domain, the equation of motion for the system is expressed as

$$\mathcal{L}(w)+\sum_{j=1}^{N_L}\mathcal{N}_j(w(\underset{\sim}{\ell}_j,t))=f \tag{1}$$

where $\mathcal{L}$ is the equation of motion of the system without the nonlinear constraint, $\mathcal{N}_j$ is the constraint force due to the j^{th} nonlinear constraint, and f is comprised of the additional forces acting on the system.

2.1 Ordinary Basis Functions

The first step in the discontinuous basis function method is to find the mode shapes of a reference system defined as

$$\mathcal{L}(w)=0 \tag{2}$$

with the same boundary conditions as the original system. For most systems this is a linear equation that can be cast in matrix-operator form [26]; that is, expressing $\mathcal{L}$ as

$$\mathcal{M}w_{,tt}+\mathcal{G}w_{,t}+\mathcal{K}w=0. \tag{3}$$

The operators $\mathcal{M}$, $\mathcal{G}$, and $\mathcal{K}$ are the mass, gyroscopic/damping, and stiffness operators respectively, and the comma subscript notation is used to denote differentiation with respect to the succeeding variables. In non-gyroscopic systems ($\mathcal{G}=0$), this modal operator notation is not strictly necessary, and more traditional modal analysis approaches may be used. Equation 3 is cast as

$$\begin{bmatrix}\mathcal{M} & 0\\ 0 & \mathcal{K}\end{bmatrix}\begin{Bmatrix}w_{,t}\\ w\end{Bmatrix}_{,t}+\begin{bmatrix}\mathcal{G} & \mathcal{K}\\ -\mathcal{K} & 0\end{bmatrix}\begin{Bmatrix}w_{,t}\\ w\end{Bmatrix}=\begin{Bmatrix}0\\ 0\end{Bmatrix}, \tag{4}$$

and has known mode shapes

$$\underset{\sim}{\Psi}_j(\underset{\sim}{x})=\underset{\sim}{\Psi}_j^R(\underset{\sim}{x})+\mathrm{i}\underset{\sim}{\Psi}_j^I(\underset{\sim}{x}) \tag{5}$$

$$\underset{\sim}{\Psi}_j^R=\begin{Bmatrix}-\omega_j\phi_j^I(\underset{\sim}{x})\\ \phi_j^R(\underset{\sim}{x})\end{Bmatrix} \tag{6}$$

$$\underset{\sim}{\Psi}_j^I=\begin{Bmatrix}\omega_j\phi_j^R(\underset{\sim}{x})\\ \phi_j^I(\underset{\sim}{x})\end{Bmatrix} \tag{7}$$

and natural frequencies ω_j. Defining the inner product of two vectors $\underset{\sim}{v}_1$ and $\underset{\sim}{v}_2$ over the domain Γ

$$\langle\underset{\sim}{v}_1,\underset{\sim}{v}_2\rangle=\int_\Gamma\underset{\sim}{v}_1^T\bar{\underset{\sim}{v}}_2\mathrm{d}\Gamma \tag{8}$$

with $\bar{\underset{\sim}{v}}$ denoting the complex conjugate of $\underset{\sim}{v}$, and the system matrices

$$\mathbb{A}=\begin{bmatrix}\mathcal{M} & 0\\ 0 & \mathcal{K}\end{bmatrix} \tag{9}$$

$$\mathbb{B}=\begin{bmatrix}\mathcal{G} & \mathcal{K}\\ -\mathcal{K} & 0\end{bmatrix}, \tag{10}$$

orthogonality yields

$$\begin{aligned}
\langle\mathbb{A}\underset{\sim}{\Psi}_m^R,\underset{\sim}{\Psi}_n^R\rangle&=\delta_{mn} & \langle\mathbb{B}\underset{\sim}{\Psi}_m^R,\underset{\sim}{\Psi}_n^R\rangle&=0\\
\langle\mathbb{A}\underset{\sim}{\Psi}_m^I,\underset{\sim}{\Psi}_n^I\rangle&=\delta_{mn} & \langle\mathbb{B}\underset{\sim}{\Psi}_m^I,\underset{\sim}{\Psi}_n^I\rangle&=0\\
\langle\mathbb{A}\underset{\sim}{\Psi}_m^R,\underset{\sim}{\Psi}_n^I\rangle&=0 & \langle\mathbb{B}\underset{\sim}{\Psi}_m^R,\underset{\sim}{\Psi}_n^I\rangle&=\omega_m\delta_{mn},
\end{aligned} \tag{11}$$

with the Kronecker delta function denoted by δ_{mn}. Since $\mathbb{B}$ is skew-symmetric

$$\langle\mathbb{B}\underset{\sim}{\Psi}_m^R,\underset{\sim}{\Psi}_n^I\rangle=-\langle\mathbb{B}\underset{\sim}{\Psi}_m^I,\underset{\sim}{\Psi}_n^R\rangle. \tag{12}$$

In the case where $\mathcal{L}$ is a nonlinear operator, such as for von Karman plates, alternative methods such as the method of quadratic components [27–29] are readily available to find the mode shapes and natural frequencies of the system. The restrictions placed on the mode shapes found by alternative methods are that they are orthonormal with respect to the system's mass matrix as above. Additionally, the number N of mode shapes needed is determined either by the highest frequency of interest for the analysis of the original system, or by a convergence study.

2.2 Discontinuous Basis Functions

A set of systems are defined that are the same as the reference system but with a linear spring at the j^{th} nonlinear constraint location; that is,

$$\mathcal{L}(w) + kw(\underset{\sim}{\ell}_j, t)\delta(\underset{\sim}{x} - \underset{\sim}{\ell}_j) = 0. \tag{13}$$

Only the first mode shape is needed for this system, and the solution can be found using the same procedure as for the reference system in Section 2.1 as the additional term $kw(\underset{\sim}{\ell}_j, t)\delta(\underset{\sim}{x} - \underset{\sim}{\ell}_j)$ is linear. The resulting set of mode shapes

$$\underset{\sim}{\Psi}_j(k, \underset{\sim}{x}) = \underset{\sim}{\Psi}_j^R(k, \underset{\sim}{x}) + \mathrm{i}\underset{\sim}{\Psi}_j^I(k, \underset{\sim}{x}) \tag{14}$$

$$\underset{\sim}{\Psi}_j^R = \begin{Bmatrix} -\varpi_j \varphi_j^I(k, \underset{\sim}{x}) \\ \varphi_j^R(k, \underset{\sim}{x}) \end{Bmatrix} \tag{15}$$

$$\underset{\sim}{\Psi}_j^I = \begin{Bmatrix} \varpi_j \varphi_j^R(k, \underset{\sim}{x}) \\ \varphi_j^I(k, \underset{\sim}{x}) \end{Bmatrix} \tag{16}$$

and corresponding natural frequencies $\varpi_j(k)$ vary as a function of the spring stiffness k. Above a critical stiffness k_c, the $\varpi_j(k)$ approach an asymptote as the linear spring acts like a pinned connection for the mode shape. To determine the discontinuous basis function, the derivative

$$\underset{\sim}{\Psi}_{j,k}(k, \underset{\sim}{x}) = \begin{Bmatrix} -\varpi_j \varphi_{j,k}^I(k, \underset{\sim}{x}) \\ \varphi_{j,k}^R(k, \underset{\sim}{x}) \end{Bmatrix} + \mathrm{i}\begin{Bmatrix} \varpi_j \varphi_{j,k}^R(k, \underset{\sim}{x}) \\ \varphi_{j,k}^I(k, \underset{\sim}{x}) \end{Bmatrix} \tag{17}$$

is needed. Note that the terms $\varpi_{j,k}\varphi_j$ are neglected as they are not necessary for deriving the discontinuous basis functions. To evaluate this derivative, an appropriate k is determined by calculating $\varpi_j(k)$ and observing where it transitions from $k \approx 0$ behavior to $k \approx \infty$ behavior. This set of functions $\{\underset{\sim}{\Psi}_{j,k}\}$ must be orthonormalized with respect to the ordinary basis functions, which can be efficiently accomplished using a Gram-Schmidt procedure resulting in the set of discontinuous basis functions

$$\begin{aligned} \underset{\sim}{\hat{\Psi}}_1 &= \underset{\sim}{\Psi}_{1,k} - \textstyle\sum_{n=1}^{N} \mathrm{proj}_{\underset{\sim}{\Psi}_n}(\underset{\sim}{\Psi}_{1,k}) \\ \underset{\sim}{\hat{\Psi}}_j &= \underset{\sim}{\Psi}_{j,k} - \textstyle\sum_{n=1}^{N} \mathrm{proj}_{\underset{\sim}{\Psi}_n}(\underset{\sim}{\Psi}_{j,k}) - \sum_{m=1}^{j-1} \mathrm{proj}_{\underset{\sim}{\hat{\Psi}}_m}(\underset{\sim}{\Psi}_{j,k}). \end{aligned} \tag{18}$$

with the projection $\mathrm{proj}_{\underset{\sim}{v}_1}(\underset{\sim}{v}_2)$ of vector $\underset{\sim}{v}_1$ on to vector $\underset{\sim}{v}_2$ is defined as

$$\mathrm{proj}_{\underset{\sim}{v}_1}(\underset{\sim}{v}_2) = \frac{\langle \underset{\sim}{v}_1, \underset{\sim}{v}_2 \rangle}{\langle \underset{\sim}{v}_1, \underset{\sim}{v}_1 \rangle} \underset{\sim}{v}_1. \tag{19}$$

After each discontinuous basis function $\underset{\sim}{\hat{\Psi}}_j$ is found it is normalized via Eq. 11, and the associated natural frequency is given as

$$\langle \mathbb{B}\underset{\sim}{\hat{\Psi}}_j^R, \underset{\sim}{\hat{\Psi}}_j^I \rangle = \hat{\omega}_j. \tag{20}$$

This complete set of basis functions $\{\underset{\sim}{\Psi}_n, \underset{\sim}{\hat{\Psi}}_m\}$ spans the entire response space. While each $\underset{\sim}{\hat{\Psi}}_m$ is at least $\mathcal{C}^1$ continuous, the third derivative (in fourth order problems) contains a discontinuity at $\underset{\sim}{x} = \underset{\sim}{\ell}_m$, which will allow for the nonlinear constraint to be accounted for. With the response of the system

$$\begin{Bmatrix} w_{,t}(\underset{\sim}{x}, t) \\ w(\underset{\sim}{x}, t) \end{Bmatrix} = \sum_{n=1}^{N} \eta_n(t)\underset{\sim}{\Psi}_n + \sum_{m=1}^{N_L} \hat{\eta}_m(t)\underset{\sim}{\hat{\Psi}}_m, \tag{21}$$

the solution of Eq. 1 is readily available. Due to the nonlinearity in the system, an implicit integration scheme is recommended. In the following examples, an implicit-explicit (IMEX) Runge-Kutta backward-Euler method [30] is used. While analytical expressions are developed for most quantities, they are not necessary for analysis by this method; numerical solutions can suffice instead of analytical expressions, however, calculating them is not as computationally efficient as analytical expressions.

3 Pinned-Pinned Beam

As an illustrative example for this method, a beam with pinned boundary conditions, having length L, position x, total displacement $w(x,t)$, boundary excitation $\Omega(t)$, and a piecewise-linear constraint that contains a deadband region located at $x = \ell$ (Fig. 1). Because this example deals with a non-gyroscopic system, modal operator notation is not necessary, and the standard, non-operator based, modal analysis is applied instead.

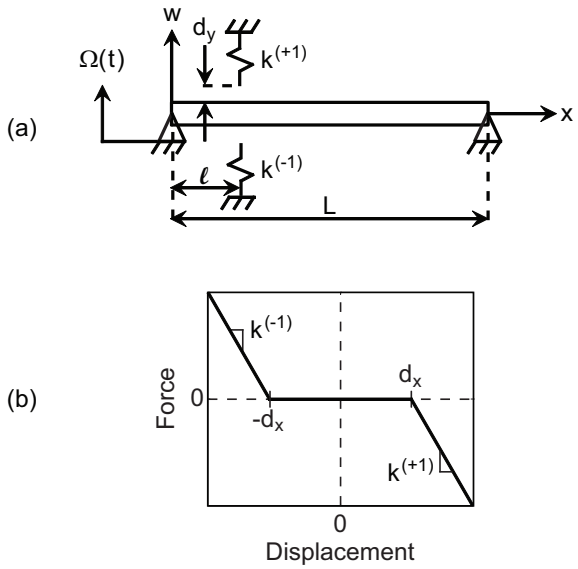

Figure 1. (a) The pinned-pinned beam system, and (b) the force-deflection profile of the deadband constraint.

The equation of motion in terms of $w(x,t)$ is

$$\rho A w_{,tt}(x,t) + EI w_{,xxxx}(x,t) = \mathcal{N}(w(\ell,t)), \tag{22}$$

where the nonlinear constraint is specified as

$$\mathcal{N}(z) = \begin{cases} k^{(-1)}(-d_x - z) & : \quad z < -d_x \\ 0 & : \quad -d_x \le z \le d_x \\ k^{(1)}(d_x - z) & : \quad d_x < z. \end{cases} \tag{23}$$

3.1 Ordinary Basis Functions

The first step in the analysis is to define the linear reference system

$$\mathcal{L}(w(x,t)) = \rho A w_{,tt}(x,t) + EI w_{,xxxx}(x,t) = 0, \tag{24}$$

which has boundary conditions

$$\begin{array}{ll} w(0,t) = \Omega(t) & w(L,t) = 0 \\ w_{,xx}(0,t) = 0 & w_{,xx}(L,t) = 0. \end{array} \tag{25}$$

In order to satisfy the inhomogeneous boundary condition, the superposition function

$$y(x,t) = \Omega(t)\left(1 - \frac{x}{L}\right) \tag{26}$$

is used. Defining the elastic displacement $u(x,t) = w(x,t) - y(x,t)$, the equation of motion is rewritten as

$$\rho A u_{,tt}(x,t) + EI u_{,xxxx} = -\rho A y_{,tt}(x,t). \tag{27}$$

Assuming the separable solution

$$u(x,t) = \sum_{n=1}^{N} \eta_n(t)\phi_n(x), \tag{28}$$

the normalized mode shapes are

$$\phi_n(x) = \sqrt{\frac{2}{\rho A L}} \sin(\lambda_n x), \tag{29}$$

with wavelengths

$$\lambda_n = \frac{n\pi}{L} \tag{30}$$

and natural frequencies

$$\omega_n = \sqrt{\frac{EI}{\rho A}}\left(\frac{n\pi}{L}\right)^2. \tag{31}$$

Substitution of (28) into (27), multiplying by $\phi_n(x)$ and integrating with respect to x yields the modal equation of motion

$$\ddot{\eta}_n(t) + \omega_n^2 \eta_n(t) = q(t). \tag{32}$$

The modal forces due to the superposition are

$$-\rho A \int_0^L \phi_n(x) y_{,tt}(x,t). \tag{33}$$

3.2 Discontinuous Basis Functions

The discontinuous basis functions are determined by first considering the system

$$\mathcal{L}(u(x,t)) + k u(\ell,t)\delta(x-\ell) = 0, \tag{34}$$

subject to pinned boundary conditions at $x = 0$ and $x = L$, with $\mathcal{L}$ defined in Eq. 24. In order to find the mode shapes of this system, it is conceptually divided into two contiguous regions (denoted by $m = 1, 2$) about $x = \ell$, and the problem is recast as

$$\mathcal{L}(u_m(x,t)) = 0, \tag{35}$$

$$\begin{array}{cc} u_1(0,t) = \Omega(t) & u_{2,xx}(0,t) = 0 \\ u_1(\ell,t) = u_2(\ell,t) & u_{1,x}(\ell,t) = u_{2,x}(\ell,t) \\ u_{1,xx}(\ell,t) = u_{2,xx}(\ell,t) & EI(u_{1,xxx}(\ell,t) - u_{2,xxx}(\ell,t)) = ku_1(\ell,t) \\ u_2(L,t) = 0 & u_{2,xx}(L,t) = 0. \end{array} \tag{36}$$

Solutions of Eqs. 35-36 are found using the separable solution

$$u_m(x,t) = \sum_{n=1}^{N} \eta_n(t)\psi_{mn}(x), \tag{37}$$

$$\begin{aligned} \psi_{mn}(x) = (&\beta_{mn1}\sin(\lambda_n x) + \beta_{mn2}\cos(\lambda_n x) \\ &+\beta_{mn3}\sinh(\lambda_n x) + \beta_{mn4}\cosh(\lambda_n x)), \end{aligned} \tag{38}$$

where λ_n is found through application of the boundary conditions and

$$\varpi_n = \sqrt{\frac{EI}{\rho A}}\lambda_n^2. \tag{39}$$

In order to determine an appropriate value of k for calculating the discontinuous basis functions, the natural frequency ϖ_n is calculated as a function of k, as shown in Fig. 2. Values of k that are too low or too high will yield discontinuous basis functions that can not adequately account for the nonlinearity in the system (either by being too soft of a constraint for low values of k or by not having any displacement at the location of the nonlinearity for high values of k). An appropriate $k \approx 0.1$ N/m (for this example, with properties listed in Table 1) is chosen from the region where ϖ transitions from a system with approximately no constraint ($k \approx 0$) to that of a pinned constraint ($k \approx \infty$). The derivative of the mode shapes $\psi_{n,k}(x)$ are numerically evaluated at the appropriate k, then orthogonalized with respect to the linear basis functions via a Gram-Schmidt procedure (18). The discontinuous basis functions $\hat{\phi}_n(x)$ are found by normalizing the orthogonal mode shapes from the Gram-Schmidt procedure with respect to the linear reference system's operators

$$\int_0^L \rho A\hat{\phi}_n(x)\hat{\phi}_j(x)\mathrm{d}x = \delta_{nj}. \tag{40}$$

In a similar manner, the corresponding natural frequency for the discontinuous basis function is found by

$$\int_0^L EI\hat{\phi}_{n,xxxx}(x)\hat{\phi}_n(x)\mathrm{d}x = \hat{\omega}_n. \tag{41}$$

In practice, only one discontinuous basis function is needed per nonlinearity; consequently, throughout the rest of this example,

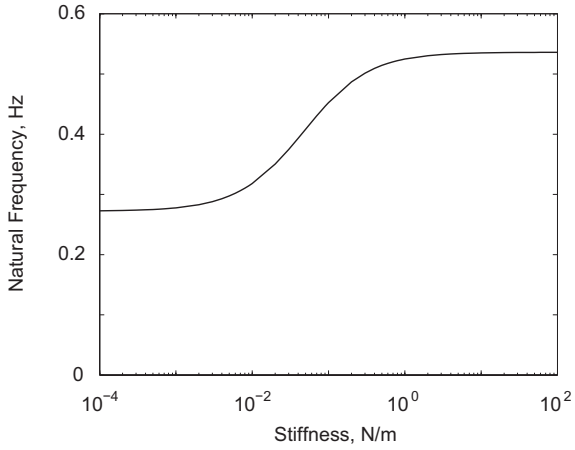

Figure 2. The natural frequency as a function of stiffness for the related problem of the reference system with a linear spring located at $x = \ell_1$.

Variable	Baseline Value
Cross-sectional area, A	0.29 mm^2
Clearance of the spring, d_x	2.5 mm
Elastic modulus, E	117 GPa
Second moment of inertia, I	0.000878 mm^4
Length of the beam, L	1 m
Contact point, l	0.25 m
Number of ordinary basis functions, N	6
Number of discontinuous basis functions, N_L	1
Beam density, ρ	11800 kg/m^3
Excitation amplitude, Ω_E	5 mm
Excitation frequency, ω_E	1 Hz

Table 1. Material and geometric properties for the pinned-pinned beam system.

only one discontinuous basis function is used. Both $\hat{\phi}_1$ and ψ_1 are shown in Fig. 3. Note that while the mode shape (Fig. 3(a)) is continuous, there is a discontinuity in the third derivative (Fig. 3(b)).

3.3 Results

Verifying that the nonlinear constraint is satisfied, the time history (Fig. 4) and phase (Fig. 5) of the beam at $x = \ell$ show that $\max(|w(\ell,t)|) \approx d_x$. The high rebound velocities and no apparent signs of steady-state behavior seen in Fig. 5 are indicative

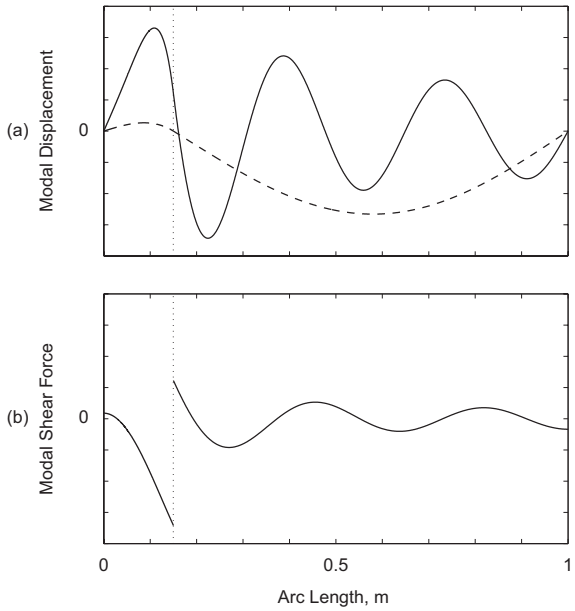

Figure 3. The (a) mode shape and (b) third derivative of the mode shape for the discontinuous basis function $\hat{\phi}_1$ (—) and the reference mode shape ψ_1 (– –) that $\hat{\phi}_1$ is derived from with $N = 5$. The location of the nonlinear constraint at $\ell = 0.15$ is indicated by the vertical dotted line, and other parameters for the system are given in Table 1.

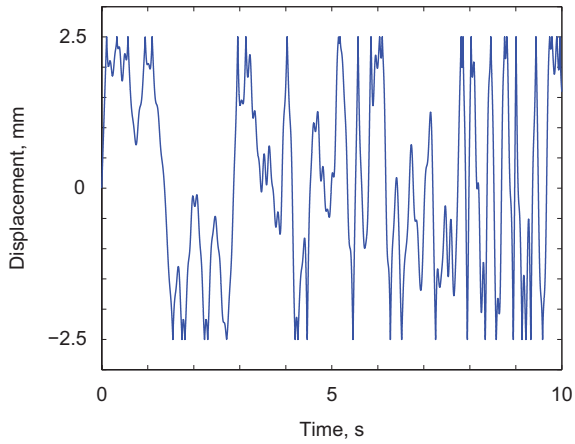

Figure 4. The time history of the displacement at $x = \ell$; parameters for the system are given in Table 1.

of the lack of damping in the system. As a result, the displacement of the beam away from the nonlinear constraint increases in magnitude with every period of the excitation. In Fig. 6, the displacement of the beam as a function of position x is shown for 50 evenly spaced time increments (each 0.15 seconds apart). Because the nonlinear constraint is located at a nodal point for

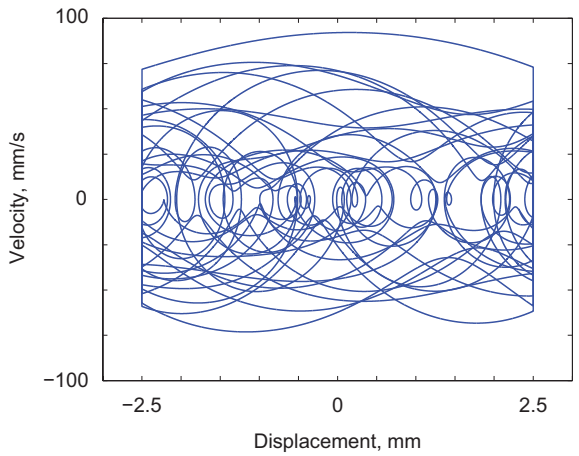

Figure 5. The phase diagram of the displacement and velocity at $x = \ell$; parameters for the system are given in Table 1.

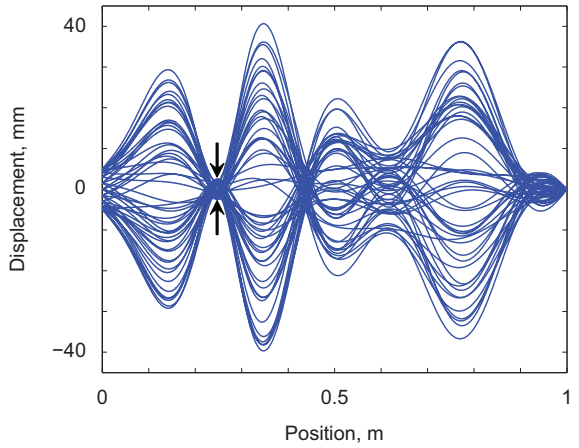

Figure 6. The displacement of the beam as a function of position at 50 evenly spaced time increments; parameters for the system are given in Table 1. The arrows indicate the location of the nonlinear constraint.

the fourth mode, the fourth mode is the dominant mode in the response.

3.3.1 Example of a Piecewise-Nonlinear Constraint To further illustrate the capabilities of the discontinuous basis function method, the force deflection profile described by

$$\mathcal{N}(z) = \begin{cases} 0.1(-d_x - z)^3 & : \quad z < -d_x \\ 0 & : \quad -d_x \le z \le d_x \\ 10^6(d_x - z) & : \quad d_x < z. \end{cases} \tag{42}$$

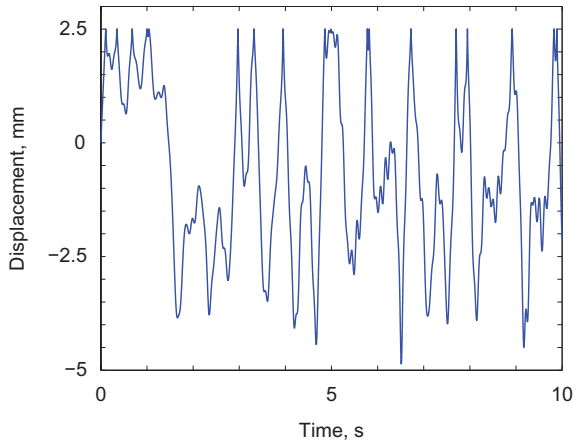

Figure 7. The time history of the displacement at $x = \ell$; parameters for the system are given in Table 1 with the constraint specified by Eq. 42.

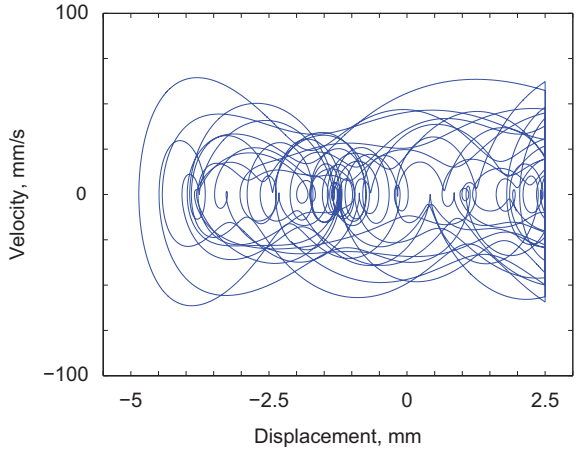

Figure 8. The phase diagram of the displacement and velocity at $x = \ell$; parameters for the system are given in Table 1 with the constraint specified by Eq. 42.

is used in place of Eq. 23 with all other parameters the same as described in Table 1. The constraint on positive displacements is still sufficiently stiff to keep $\max(w(\ell,t)) \approx d_x$; however, because the constraint on negative displacements is significantly less stiff, displacements of $w(\ell,t) < -d_x$ are observed in both the time history (Fig. 7) and phase diagram (Fig. 8). Even though the constraint was changed from a piecewise-linear to a piecewise-nonlinear function, no new basis functions or discontinuous basis functions need to be calculated; the same basis functions as derived for the piecewise-linear constraint are used with no more calculations than for the piecewise-linear constraint.

Figure 9 shows the displacement of the beam as a function of x at 50 evenly spaced time increments (each 0.15 seconds apart). Despite the change in the nonlinear constraint, the displacement of the beam is qualitatively similar to the previous example with the piecewise-linear constraint (Fig. 6). This reinforces the observation that many different constraint models can be expressed as limiting cases of piecewise-linear models [14, 31–33] provided that approximately the same stiffness is used as compared to the system. Even in this example, where the stiffness of the constraint on negative displacements is much less than in the piecewise-linear case, the displacement of the beam is still qualitatively the same away from the location of the constraint.

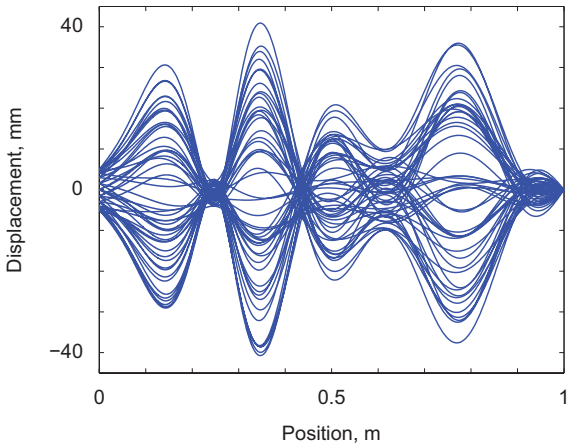

Figure 9. The displacement of the beam as a function of position at 50 evenly spaced time increments; parameters for the system are given in Table 1 with the constraint specified by Eq. 42.

The constraint force as a function of time is shown in Fig. 10.

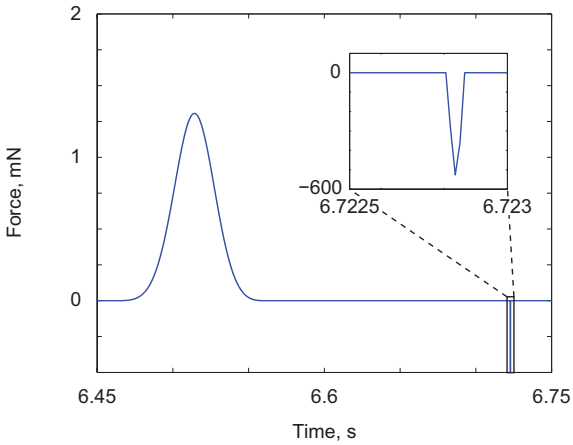

Figure 10. The constraint force as a function of time; parameters for the system are given in Table 1 with the constraint (42). The inset shows a magnification of the constraint force for $6.7225 \le t \le 6.723$ s.

Because the constraint for positive displacements is much stiffer than for negative displacements, the forces must be plotted on separate scales for clarity. Despite a relatively coarse time step (as indicated by the non-smooth nature of the constraint force shown in the inset), the constraint on positive displacements is still adequately modeled. This is significant because the main constraint on computational time for this method is time step size. Since the discontinuous basis function method does not map from one state of the constraint to another (such as in the exact methods of [5, 20, 23]), the exact time of contact between the beam and the nonlinear constraint is not required.

3.3.2 Extension to Multiple Constraints Previously, only one constraint has been considered. In extending the discontinuous basis function method to multiple constraints, only one additional discontinuous basis function is needed for each additional constraint. These new discontinuous basis functions must be normalized with respect to the other basis functions; beyond this, though, no additional calculation are needed. In Fig. 11, four nonlinear constraints (located at $\ell_1 = 0.2$ m, $\ell_2 = 0.4$ m, $\ell_3 = 0.6$ m, and $\ell_4 = 0.8$ m) are modeled with the constitutive relationship described in Eq. 23.

The effect of the additional constraints is to significantly attenuate the magnitude of the displacement along the entire length of the beam, not just at the location of the constraints. Additionally, every time a constraint is contacted, a sharp change in the velocity is seen along the beam. This is particulary evident in the phase diagram for the displacement and velocity of the beam at $x = \ell_1$ (Fig. 12). As a result, high frequency motion is observed as waves traveling along the beam due to contact with the constraints.

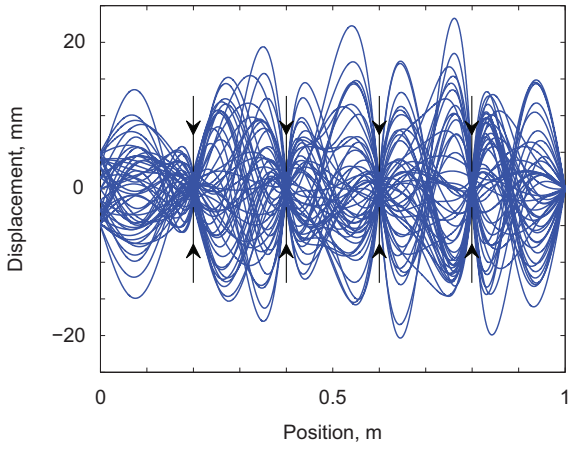

Figure 11. The displacement of the beam as a function of position at 50 evenly spaced time increments; parameters for the system are given in Table 1 with constraints located at $\ell_1 = 0.2$ m, $\ell_2 = 0.4$ m, $\ell_3 = 0.6$ m, and $\ell_4 = 0.8$ m. The arrows and thin lines indicate the location of the nonlinear constraints.

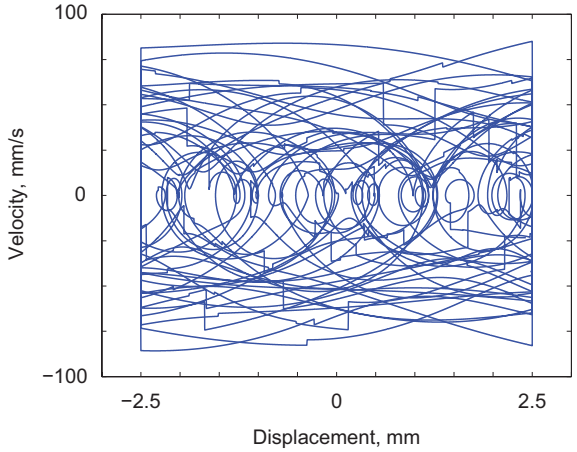

Figure 12. The phase diagram of the displacement and velocity at $x = \ell$; parameters for the system are given in Table 1 with constraints located at $\ell_1 = 0.2$ m, $\ell_2 = 0.4$ m, $\ell_3 = 0.6$ m, and $\ell_4 = 0.8$ m.

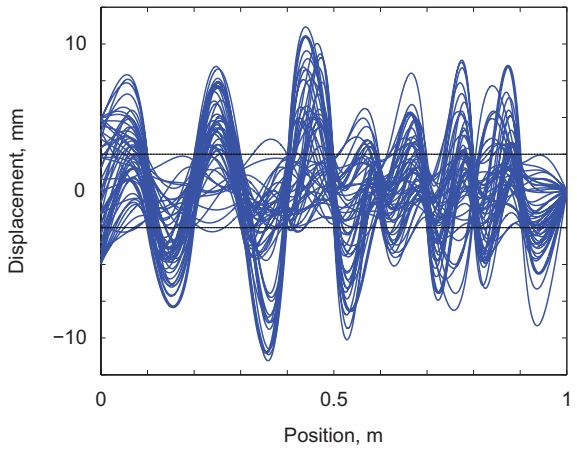

Figure 13. The displacement of the beam as a function of position at 50 evenly spaced time increments; parameters for the system are given in Table 1 with constraints located at $\ell_n = 0.1n$ m, $n = 1, 2, \ldots, 9$. Dashed lines indicate the deadband region ($-d_x \le w(\ell_n, t) \le d_x$) of the nonlinear constraints.

In Fig. 13, the number of constraints is further increased to 9 (located at $\ell_n = 0.1n$ m, $n = 1, 2, \ldots, 9$). The displacement is significantly attenuated along the length of the beam, and the response is no longer approximately symmetric about $w(x,t) = 0$ (as in Figs. 6 and 11).

4 Conclusions

A new method for analyzing discrete, nonlinear constraints in continuous systems is developed. This method approximately solves for the state of the system by using discontinuous basis functions to account for the nonlinear constraints. These discontinuous basis functions are used to supplement the linear basis functions (eigen modes) of the system. While the discontinuous basis functions are continuous in displacement, their higher derivatives contain discontinuities. Unlike exact methods that are limited to piecewise-linear constraints, this new method of discontinuous basis functions neither divides the system into multiple regimes based on the constraints, nor requires the exact time of engagement of a nonlinear constraint. Additionally, the only assumption placed on the nonlinear constraint is that it can be modeled in a discrete manner. An illustrative example of a pinned-pinned beam is used to demonstrate the application of this method. Both piecewise-linear and piecewise-nonlinear constraints are modeled, and the number of constraints used in the illustrative results are varied from one to nine. The primary conclusions of this work are

1. The discontinuous basis function method is a robust and efficient technique for modeling the effects of nonlinear constraints on continuous systems. The advantage of this method lies in not needing separate sets of basis functions for each regime of the constraints, and not needing to find the precise times that different regimes of the constraints are engaged.
2. Changing the constitutive properties of the nonlinear constraint, such as from a linear spring to a piecewise-linear constraint or to a piecewise-nonlinear constraint, requires no additional calculations as the discontinuous basis function method is derived independent of the constraint model.
3. Only one discontinuous basis function is needed for each nonlinear constraint. Thus, extension of the method to multiple constraints requires only one additional discontinuous basis function for each additional constraint.
4. Results from analyzing a pinned-pinned beam shows that qualitatively similar behavior is observed for both piecewise-linear and piecewise-nonlinear constraints; however, the forces and displacements at the constraint location may differ significantly. Further analysis of this observation is an area for future work.

Acknowledgements

We would like to thank our colleagues Michael J. Starr and Jamey T. Bond for their constructive feedback on drafts of this paper.

REFERENCES

[1] Wilson, J. F., and Callis, E. G., 2004. "The dynamics of loosely jointed structures". *International Journal of Non-Linear Mechanics,* ***39***, pp. 503–514.

[2] Sarkar, S., and Dattaguru, K. V. B., 2004. "Dynamics of flexible structures with nonlinear joints". *ASME Journal of Vibration and Acoustics,* ***126***, pp. 92–100.

[3] Kahraman, A., 2001. "A spline joint formulation for drive train torsional dynamic models". *Journal of Sound and Vibration,* ***241***, pp. 328–336.

[4] Natsiavas, S., Theodossiades, S., and Goudas, I., 2000. "Dynamic analysis of piecewise linear oscillators with time periodic coefficients". *International Journal of Non-Linear Mechanics,* ***35***, pp. 53–68.

[5] Ervin, E. K., and Wickert, J. A., 2007. "Repetitive impact response of a beam structure subjected to harmonic base excitation". *Journal of Sound and Vibration,* ***307***, pp. 2–19.

[6] Luo, G. W., Zhang, Y. L., and Zhang, J. G., 2006. "Dynamical behavior of a class of vibratory systems with symmetrical rigid stops near the point of codimension two bifurcation". *Journal of Sound and Vibration,* ***297***, pp. 17–36.

[7] Zuo, L., and Curnier, A., 1994. "Non-linear real and complex modes of conewise linear systems". *Journal of Sound and Vibration,* ***174***, pp. 289–313.

[8] Aoki, S., and Watanabe, T., 2000. "Analytical method of response of piping system with nonlinear support". *ASME Journal of Pressure Vessel Technology,* ***122***, pp. 437–442.

[9] Qiao, N., Lin, W., and Qin, Q., 2006. "Bifurcations and chaotic motions of a curved pipe conveying fluid with nonlinear constraints". *Computers and Structures,* ***84***, pp. 708–717.

[10] Hemsel, T., Stroop, R., Uribe, D. O., and Wallaschek, J., 2007. "Resonant vibrating sensors for tactile tissue differentiation". *Journal of Sound and Vibration,* ***308***, pp. 441–446.

[11] Aoki, S., and Watanabe, T., 2006. "An investigation of an impact vibration absorber with hysteresis damping". *ASME Journal of Pressure Vessel Technology,* ***128***, pp. 508–515.

[12] Jerrelind, J., and Stensson, A., 2000. "Nonlinear dynamics of parts in engineering systems". *Chaos, Solitons and Fractals,* ***11***, pp. 2413–2428.

[13] Wiercigroch, M., 2000. "Modelling of dynamical systems with motion dependent discontinuities". *Chaos, Solitons and Fractals,* ***11***, pp. 2429–2442.

[14] Foale, S., and Bishop, S. R., 1994. "Bifurcations in impact oscillations". *Nonlinear Dynamics,* ***6***, pp. 285–299.

[15] van de Vorst, E. L. B., van Campen, D. H., and de Kraker, A., 1996. "Periodic solutions of a multi-dof beam system with impact". *Journal of Sound and Vibration,* ***192***, pp. 913–925.

[16] van de Wouw, N., de Kraker, A., van Campen, D. H., and

Nijmeijer, H., 2003. "Non-linear dynamics of a stochastically excited beam system with impact". *International Journal of Non-Linear Mechanics,* ***38***, pp. 767–779.

[17] Païdoussis, M. P., and Li, G. X., 1992. "Cross-flow-induced chaotic vibrations of heat-exchanger tubes impacting on loose supports". *Journal of Sound and Vibration,* ***152***, pp. 305–326.

[18] Segalman, D. J., 2005. "A four-parameter Iwan model for lap-type joints". *ASME Journal of Applied Mechanics,* ***72***, pp. 752–760.

[19] Tangpong, X. W., Wickert, J. A., and Akay, A., 2008. "Distributed friction damping of travelling wave vibration in rods". *Philosophical Transactions of the Royal Society of London A,* ***366***, pp. 811–827.

[20] Brake, M. R., and Wickert, J. A., 2010. "Modal analysis of a gyroscopic system with nonlinear constraints". *Journal of Sound and Vibration,* ***329***, pp. 893–911.

[21] Metallidis, P., and Natsiavas, S., 2000. "Vibration of a continuous system with clearance and motion constraints". *International Journal of Non-Linear Mechanics,* ***35***, pp. 675–690.

[22] Fegelman, K. J. L., and Grosh, K., 2004. "Dynamics of a flexible beam contacting a linear spring at low frequency excitation: Experiment and analysis". *ASME Journal of Vibration and Acoustics,* ***124***, pp. 237–249.

[23] Brake, M. R., submitted. "A hybrid approach for the modal analysis of continuous systems with nonlinear constraints". *Journal of Sound and Vibration*.

[24] Milman, M. H., and Chu, C.-C., 1994. "Optimization methods for passive damper placement and tuning". *Journal of Guidance, Control, and Dynamics,* ***17***, pp. 848–856.

[25] Segalman, D. J., 2007. "Model reduction of systems with localized nonlinearities". *ASME Journal of Computational and Nonlinear Dynamics,* ***2***, pp. 249–266.

[26] Wickert, J. A., and Mote, Jr., C. D., 1990. "Classical vibration analysis of axially moving continua". *ASME Journal of Applied Mechanics,* ***57***, pp. 738–744.

[27] Segalman, D. J., and Dohrmann, C. R., 1996. "A method for calculating the dynamics of rotating flexible structures, part 1: Derivation". *ASME Journal of Vibration and Acoustics,* ***118***, pp. 313–317.

[28] Segalman, D. J., Dohrmann, C. R., and Slavin, A. M., 1996. "A method for calculating the dynamics of rotating flexible structures, part 2: Example calculations". *ASME Journal of Vibration and Acoustics,* ***118***, pp. 318–322.

[29] Brake, M. R., and Segalman, D. J., 2010. "Nonlinear model reduction of von Karman plates under quasi-steady fluid flow". *AIAA Journal,* ***48***, pp. 2339–2347.

[30] Ascher, U. M., Ruuth, S. J., and Spiteri, R. J., 1997. "Implicit-explicit Runge-Kutta methods for time-dependent partial differential equations". *Applied Numerical Mathematics,* ***25***, pp. 151–167.

[31] Wang, C., and Kim, J., 1996. "New analysis method for a thin beam impacting against a stop based on the full continuous model". *Journal of Sound and Vibration,* ***191***, pp. 809–823.

[32] Shaw, S. W., and Holmes, P. J., 1983. "A periodically forced piecewise linear oscillator". *Journal of Sound and Vibration,* ***90***, pp. 129–155.

[33] Todd, M. D., and Virgin, L. N., 1996. "Natural frequency considerations of an impact oscillator". *Journal of Sound and Vibration,* ***194***, pp. 452–460.